A conserved photosynthetic cytochrome enhances growth in fluctuating light

Darius Kosmützky[1,‡,*], Laura T Wey[2], Lauri Nikkanen[2], Aron Ferenczi[3], Joshua M Lawrence[1,4], Alberto Scarampi[1,‡‡], Attila Molnar[3], Yagut Allahverdiyeva[2], Christopher J Howe[1,*]

1: Department of Biochemistry, University of Cambridge, Cambridge CB2 1QW, UK

2: Molecular Plant Biology, Department of Life Technologies, University of Turku, Turku 20014, Finland

3: Institute of Molecular Plant Sciences, University of Edinburgh, Edinburgh EH9 3BF, UK

4: Yusuf Hamied Department of Chemistry, University of Cambridge, Cambridge CB2 1EW, UK

‡: Present address: Sainsbury Laboratory, University of Cambridge, Cambridge CB2 1LR, UK

‡‡: Present address: School of Life Sciences, University of Warwick, Coventry CV4 7AL, UK

*: Corresponding authors

Abstract

Having at least one of the small soluble electron carriers cytochrome c_6 (c_6) and plastocyanin is indispensable for photosynthesis. It was believed that c_6 had been lost from plants until the identification of a ubiquitous and highly conserved homologue, now named cytochrome c_{6A} (c_{6A}), led to a paradigm shift. However, c_{6A} was soon shown to be unable to replace c_6 (or plastocyanin) functionally in the photosynthetic electron transport chain, despite their significant structural homology. The function of c_{6A}, and why it is apparently universal in plants and green algae, remain unknown. Here, we show that, in the green alga *Chlamydomonas reinhardtii*, c_{6A} confers a growth advantage under fluctuating light and is crucial for maintaining the light harvesting balance between photosystems I and II in photomixotrophic conditions. We show that in the absence of c_{6A}, the light harvesting balance shifts towards PSII, leading to a more reduced plastoquinone pool and increased photooxidative stress. This study provides new insights into how photosynthetic organisms acclimatize to stressful light conditions, indicating that c_{6A} is important for this adaptation. These findings provide a basis for further mechanistic studies on a hypothesized role for c_{6A} in thiol-based redox regulation in the thylakoid lumen, with implications for photoprotection mechanisms such as state transitions.

Introduction

The photosynthetic electron transport chain (PETC) is essential for nearly all life on Earth (Fig. 1a). At least one of the soluble electron carriers plastocyanin and cytochrome c_6 is indispensable for the PETC to function (1, 2). A close homologue of c_6, cytochrome c_{6A}, was first discovered in *Arabidopsis thaliana* and later in other plants and eukaryotic algae (3, 4). Whereas plants lost the gene for c_6 and contain only c_{6A}, some eukaryotic algae such as *Chlamydomonas reinhardtii* (*Chlamydomonas*) contain genes for both (5), although c_{6A} is expressed at a low level compared to c_6 or plastocyanin (6, 7). Since its discovery, c_{6A} has been hypothesized to have various functions, including replacement of plastocyanin (3), acting as a safety valve for excess electrons of photosynthesis (7), regulation of generation of reactive oxygen species (ROS) in PSI (8), and being involved in high light signalling (9) or thiol-based redox regulation (10, 11). However, the function of cytochrome c_{6A} remains elusive (7).

While c_6 and c_{6A} are homologues, there are structural differences between the two (Fig. 1b). c_{6A} contains a 'loop insertion peptide' (LIP), an insertion with a conserved disulfide bridge in a surface-located and well-defined loop. The LIP is absent from c_6 (10). Assessing the stability of various mutant proteins showed that the LIP is structurally important (12, 13). While a catalytic role for the conserved disulfide bridge within the LIP is uncertain, it is predicted to contribute to the protein's structural stability(13, 14). Furthermore, differences in heme environment contribute to c_{6A} (+71 mV (15)) having a 254 mV more negative midpoint potential than plastocyanin or c_6 (+325 mV (15)).

Phylogenetic analyses revealed that c_{6A} represents a monophyletic group distinct from c_6 and likely originates from cyanobacterial cytochrome c_{6B}, another homologue of c_6 that has a similar midpoint potential to c_{6A} but lacks the LIP (16). The sequence of c_{6A} is highly conserved across the green lineage, as with plastocyanin, suggesting an important role for c_{6A} within photosynthetic eukaryotes (16). However, the large difference in midpoint potentials renders it highly unlikely that c_{6A} acts as a functional replacement for plastocyanin in plants and algae, as the former cannot accept electrons from the cytochrome b_6f complex (Fig. 1a). Further, plastocyanin was found to be indispensable even when c_{6A} was overexpressed in *A. thaliana*[1]. Additionally, the surfaces of c_6 and plastocyanin are strongly negatively charged, whereas c_{6A} has a strongly positive surface charge (17). Together with the difference in isoelectric points (plastocyanin: 5.1, c_{6A}: 4.1 in *A. thaliana* (18)) this indicates different interactions.

Interactions involving c_{6A} further highlight its distinct role (Fig. 1a). It cannot effectively reduce PSI *in vitro*, making direct interaction between c_{6A} and PSI unlikely (17). Additionally, c_{6A} has been shown to reduce plastocyanin *in vitro* (19) and weak interaction (K_d = 2.01 mM) was detected with plastocyanin using NMR titrations (6), consistent with a transient interaction. Yeast Two-Hybrid

assays also revealed interactions of c_{6A} with itself (20), the lumen thiol oxidase LTO1 (21), and the redox-regulated immunophilin FKBP13 (3). For LTO1 an involvement in regulating state transitions via the kinase STT7 has been described (22). Interaction with LTO1 and FKBP13 suggests a luminal localization for c_{6A}, consistent with its detection in the soluble fraction of the thylakoid lumen in *A. thaliana* (23). In *Chlamydomonas*, however, only chloroplastic localization has been confirmed (6). In *A. thaliana*, c_{6A} was also found to be uniquely localized to sensory plastids in the epidermis and vascular parenchyma rather than mesophyll chloroplasts (24).

Photosynthetic organisms require flexibility in their photosynthetic apparatus because they grow under a diverse set of environmental conditions. These include varying light conditions from diurnal cycles to more rapid fluctuations caused by the sun, clouds, canopy, and in the case of *Chlamydomonas*, also soil and water movements. For *Chlamydomonas*, exposure to a 12 s on/12 s off cycle with light intensities of 600-700 µmol photons m^{-2} s^{-1} in photoautotrophic conditions resulted in growth rates reaching only about 30% of those achieved under continuous illumination (25). Additionally, a growth penalty was revealed under fluctuating light with frequencies in the range of 10-100 s on/off (26). In mutant assays using *Chlamydomonas*, various fluctuating light regimes have been employed to determine the function of proteins associated with photosynthesis. Prominent members include Proton Gradient Regulation 5 (PGR5) and Proton Gradient Regulation Like 1 (PGRL1) proteins, both implicated in cyclic electron flow, its regulation or ATP synthase regulation (27), as well as flavodiiron proteins (FLVA/B), which facilitate the Mehler-like reaction (28). Additionally, the qE quenching effector LHCSR3 (29, 30) and plastid terminal oxidase PTOX2 (31) have been implicated in the response to fluctuating light, as mutants of all of these proteins showed a growth deficit under fluctuating light conditions.

Here, we present the first in-depth analysis of the connection between c_{6A} and photosynthesis. We show that this highly conserved protein is important for growth under a harsh fluctuating light regime we called DISCO Light and helps maintain the redox balance of the plastoquinone (PQ) pool through its effect on the light harvesting balance between photosystems I (PSI) and II (PSII).

Results

<u>Cytochrome c_{6A} confers a growth advantage under a fluctuating light regime</u>

To investigate the role of c_{6A} in *Chlamydomonas* we used CRISPR/Cpf1 (32) to create a knock-out of the c_{6A} gene (*CYC4*, Cre16.g670950) in the background strain CC-1883 (WT). The knock-out strain ("c_{6A}-KO") was confirmed through PCR and sequencing (Methods & Supplementary Fig. 1a-d). We also generated a c_{6A} overexpression (c_{6A}-OE) strain by transforming the c_{6A}-KO strain with a construct

that drives the expression of FLAG-tagged c_{6A} from a *PSAD* promoter. Overexpression was confirmed by immunoblot and RNAseq analysis (Methods & Supplementary Fig. 1d-e).

To investigate the role of cytochrome c_{6A} in growth, we tested how *Chlamydomonas* strains grow under various light and trophic regimes. Under continuous light (30 µmol photons m^{-2} s^{-1}), both c_{6A}-KO and WT strains reached similar maximum optical densities (OD_{750nm}) of around 2 in photomixotrophic and ~0.6 in photoautotrophic conditions, with no statistically significant differences (Fig. 1c). We defined continuous light (30 µmol photons m^{-2} s^{-1}) and photomixotrophic conditions as standard conditions for this study.

We also tested multiple stressful light conditions for their effect on c_{6A}-KO and WT. Only a novel light regime we named DISCO (Darkness Interrupted by Short COnstant) Light and photomixotrophy led to an observable phenotypic growth difference (Fig. 1c). DISCO Light was devised to expose *Chlamydomonas* to a complex fluctuating light regime covering multiple frequencies, as it consists of two alternating phases: 2 min of darkness followed by 2 min of alternating 12 s high light pulses of 700 $\mu mol_{photons}$ m^{-2} s^{-1} and 12 s darkness (Fig. 1d). c_{6A}-KO grew more slowly and reached lower cell densities than WT under photomixotrophic DISCO conditions (Fig. 1c & e): after one day c_{6A}-KO cultures showed significantly reduced growth ($P = 0.029$), and by day 3 they were approximately 1.5 times less dense than WT cultures ($P = 0.10$). The growth penalty in c_{6A}-KO was recovered by overexpressing c_{6A}, with c_{6A}-OE showing significantly higher cell densities than c_{6A}-KO from day 1 ($P = 0.024$, Fig. 1c & e). In the DISCO light regime without acetate in the medium (photoautotrophy), no strain could grow (Supplementary Fig. 2e).

In photomixotrophy and darkness or continuous high light at the same light intensity as in the DISCO regime (700 $\mu mol_{photons}$ m^{-2} s^{-1}) WT and c_{6A}-KO grew at similar rates (Supplementary Fig. 2a-b). Furthermore, fluctuating light regimes corresponding to elements of the DISCO protocol ("2 min high light & 2 min darkness", and "12 s high light & 12 s darkness"), showed only small differences between WT and c_{6A}-KO that were not part of a consistent trend under either photomixotrophic or photoautotrophic conditions (Supplementary Fig. 2c-d).

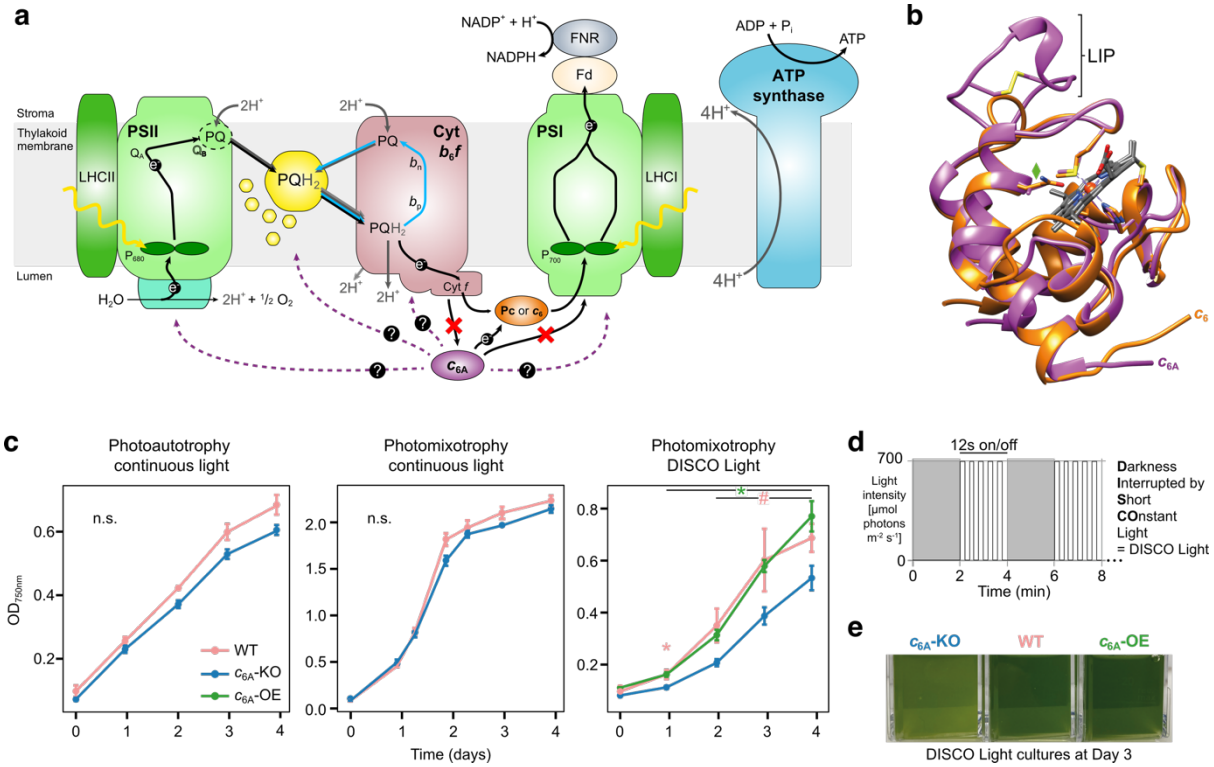

Figure 1: Cytochrome c_{6A} confers a growth advantage under a fluctuating light regime. a, Schematic of the photosynthetic electron transport chain with known (black) and putative interactions (purple) of c_{6A} marked. Proton movement (grey) and the Q-cycle (blue) are shown as arrows. **b**, Overlay of the crystal structures of cytochrome c_6 from *Chlamydomonas* (orange, PDB: 1CYJ (33)) and c_{6A} from *A. thaliana* (purple, PDB: 2CE0 (19)). The position of the LIP is noted with the disulfide bridge formed between the two conserved cysteine residues (yellow sticks). The amino acid residues at position 52 were found to affect the heme environment contributing to the low midpoint potential of c_{6A} compared to c_6 or plastocyanin (stick model and labelled with a green diamond) (15). **c**, Optical density (OD_{750nm}) growth curve of c_{6A} mutant strains and WT under continuous light (30 $\mu mol_{photons}\ m^{-2}\ s^{-1}$) in either photoautotrophy or -mixotrophy and DISCO Light and photomixotrophy (n = 3 biological replicates ±SD). Statistical testing was carried out with repeated measures ANOVA. Post hoc pairwise two-sided t-tests at each time point were performed if the interaction effect of time and strain on OD_{750nm} in the ANOVA was significant ($p_{time:strain} < 0.05$) comparing WT (pink) or c_{6A}-OE (green) against c_{6A}-KO ($p < 0.05$: *, $p \leq 0.1$: #). **d**, DISCO Light (Darkness Interrupted by Short COnstant Light) consists of alternating 2 min darkness followed by 2 min of high light pulses (12 s high light (700 $\mu mol_{photons}\ m^{-2}\ s^{-1}$) & 12 s darkness). **e**, Visual differences of the c_{6A} mutant and WT cultures of at day 3 of growth in DISCO Light.

Measurements of total chlorophyll concentration and acetate consumption confirmed the phenotypic difference between the strains observed from OD_{750nm} measurements in both standard and DISCO Light conditions (Supplementary Fig. 2f-h). The correlation between total chlorophyll concentration and optical density was similar between WT and c_{6A}-KO. This indicated no difference in chlorophyll concentration per cell between the strains under standard conditions or DISCO Light (Supplementary Fig. 2g). Additionally, measurements of acetate concentration in the growth medium indicated that c_{6A}-KO consumed less acetate, likely because of lower cell densities when exposed to DISCO Light, with differences apparent from day 3 (Supplementary Fig. 2h).

These results indicate that c_{6A} is important for growth of *Chlamydomonas* under the high intensity and rapidly fluctuating DISCO Light regime and acetate availability in photomixotrophic conditions.

155 c_{6A} is likely localized in the thylakoid lumen and does not have strongly bound interaction partners
156 c_{6A} was detected in the soluble fraction of the thylakoid lumen in *A. thaliana* (23). In
157 *Chlamydomonas*, however, only chloroplastic localization has been confirmed (6). To determine the
158 subcellular localization of c_{6A} in *Chlamydomonas* further, we performed immunofluorescence
159 microscopy on the c_{6A}-FLAG overexpressing strain (c_{6A}-OE) and its background strain (c_{6A}-KO)
160 grown under standard conditions. In the negative control (c_{6A}-KO), the AlexaFluor488 signal
161 corresponding to FLAG was weak and non-specific, i.e. appearing throughout the cell including in the
162 flagella (Supplementary Fig. 3a). In contrast, the c_{6A}-FLAG overexpressing sample (c_{6A}-OE) showed
163 a more intense (2 to 3-fold pixel intensity) and more localized fluorescence signal, confirming
164 chloroplast-specific localization of c_{6A} (Supplementary Fig. 3b). Two cells covering the variation of
165 AlexaFluor488 signal intensity were chosen as representatives to capture cell to cell differences that
166 could arise from technical variation from fixing and staining or c_{6A}-FLAG expression level
167 differences between cells. Nevertheless, the absence of AlexaFluor488 signal from cell compartments
168 other than the chloroplast in c_{6A}-OE compared to c_{6A}-KO supports the FLAG-specificity of the signal.
169 The detection of anti-FLAG signal in structures resembling pyrenoid-traversing thylakoids supports a
170 thylakoid luminal localization of the soluble c_{6A} (Supplementary Fig. 3c-d). While it cannot be
171 excluded that c_{6A} is associated with the thylakoid membrane on the stromal side, the structure of c_{6A}
172 (Fig. 1b) gives no indication of membrane-association.

173 To detect possible covalent or strongly bound interaction partners, we performed co-
174 immunoprecipitation (co-IP) analyses of the c_{6A}-FLAG overexpressing strain (c_{6A}-OE) and the
175 untransformed background strain (c_{6A}-KO) using anti-FLAG-agarose beads. Immunodetection of
176 FLAG in the precipitate revealed bands at ~15 kDa in c_{6A}-OE but not in c_{6A}-KO, corresponding to
177 mature c_{6A}-FLAG (red arrows in Supplementary Fig. 4), with additional FLAG signals that were not
178 c_{6A}-FLAG specific in the 25-35 kDa range (black arrows in Supplementary Fig. 4). Under both
179 standard (Supplementary Fig. 4c) and DISCO Light (Supplementary Fig. 4f) conditions, the
180 immunoprecipitate did not reveal any bands unique to c_{6A}-OE except the c_{6A}-FLAG band, indicating
181 that no specific interaction partners of c_{6A} were detected.

182 The combined immunofluorescence microscopy and co-IP results indicate that c_{6A} is likely to be
183 localized in the thylakoid lumen and are consistent with any hypothesized function relying primarily
184 on weak or transient interactions.

185

186 c_{6A} is important to maintain the light harvesting balance between photosystems I and II in
187 photomixotrophy
188 Given the light-dependent growth phenotype observed in DISCO conditions, the likely localization of
189 c_{6A} in the thylakoid lumen, and c_{6A}'s high sequence similarity to c_6 which is involved in the PETC, we

190 investigated the photosystems and light harvesting complexes to explore further a potential role of c_{6A}
191 in photosynthesis.

192 We recorded low temperature (77K) chlorophyll fluorescence emission spectra. When grown in
193 continuous light (30 $\mu mol_{photons}$ m^{-2} s^{-1}) under photoautotrophic conditions WT and c_{6A}-KO exhibited
194 very similar fluorescence spectra (Fig. 2a, PSI/PSII fluorescence ratios 1.25 and 1.3, respectively, P =
195 0.374), consistent with similar growth (Fig. 1c). However, when grown in photomixotrophic
196 conditions and continuous light (30 $\mu mol_{photons}$ m^{-2} s^{-1}, standard conditions), and despite the two
197 strains showing similar growth (Fig. 1b), WT maintained a PSI/PSII fluorescence ratio of about 1.2,
198 while c_{6A}-KO showed a significantly lower ratio (0.96, P = 0.008), which was accompanied by a more
199 prominent CP47-associated peak at 695 nm (34) (Fig. 2a). The PSI/PSII fluorescence ratio was
200 restored to nearly WT levels in the c_{6A}-OE strain (Fig. 2a). When samples were grown in DISCO
201 Light and photomixotrophy, the differences seen in standard conditions were amplified. By day 4, the
202 PSI/PSII fluorescence ratio in c_{6A}-KO dropped drastically to 0.66 in comparison to WT and c_{6A}-OE
203 (1.05 and 1.33, respectively & P = 0.027 and 0.0005, respectively). Interestingly, WT showed a
204 shoulder peak at ~681 nm (Fig. 2a), which may reflect partial detachment of light harvesting complex
205 II (LHCII) from PSII (35). The lower level of normalized PSI fluorescence in c_{6A}-KO in all
206 photomixotrophic samples did not originate from lower PSI protein levels, as evidenced by PSI
207 subunit immunoblot analyses (Supplementary Fig. 5).

208 To investigate if this c_{6A}-dependent light harvesting phenotype was due to alterations in state
209 transitions in photomixotrophy, for example due to c_{6A}-KO being locked in state 1, we induced either
210 state 1 (darkness and oxia) or state 2 (darkness and anoxia) in samples grown under standard
211 conditions (Fig. 2b). Both strains showed, as expected, a lower PSI/PSII fluorescence ratio in state 1
212 and a higher PSI/PSII fluorescence ratio in state 2, reflecting the increased sizes of the antenna cross
213 section of PSII and PSI, respectively. However, c_{6A}-KO consistently exhibited a lower PSI/PSII
214 fluorescence ratio than WT (Fig. 2c). Whereas WT exhibited PSI fluorescence of 1.13 (normalized to
215 PSII fluorescence) in state 2 conditions, c_{6A}-KO showed a significantly lower value of 1.01 (P =
216 0.046). Similarly, under state 1 inducing conditions, normalized PSI fluorescence in WT was 0.85,
217 compared to 0.77 in c_{6A}-KO (P = 0.071). While the CP47-associated peak at 695 nm (34) showed
218 different intensity between the two states in WT, in c_{6A}-KO the same peak intensity was recorded in
219 both states.

220

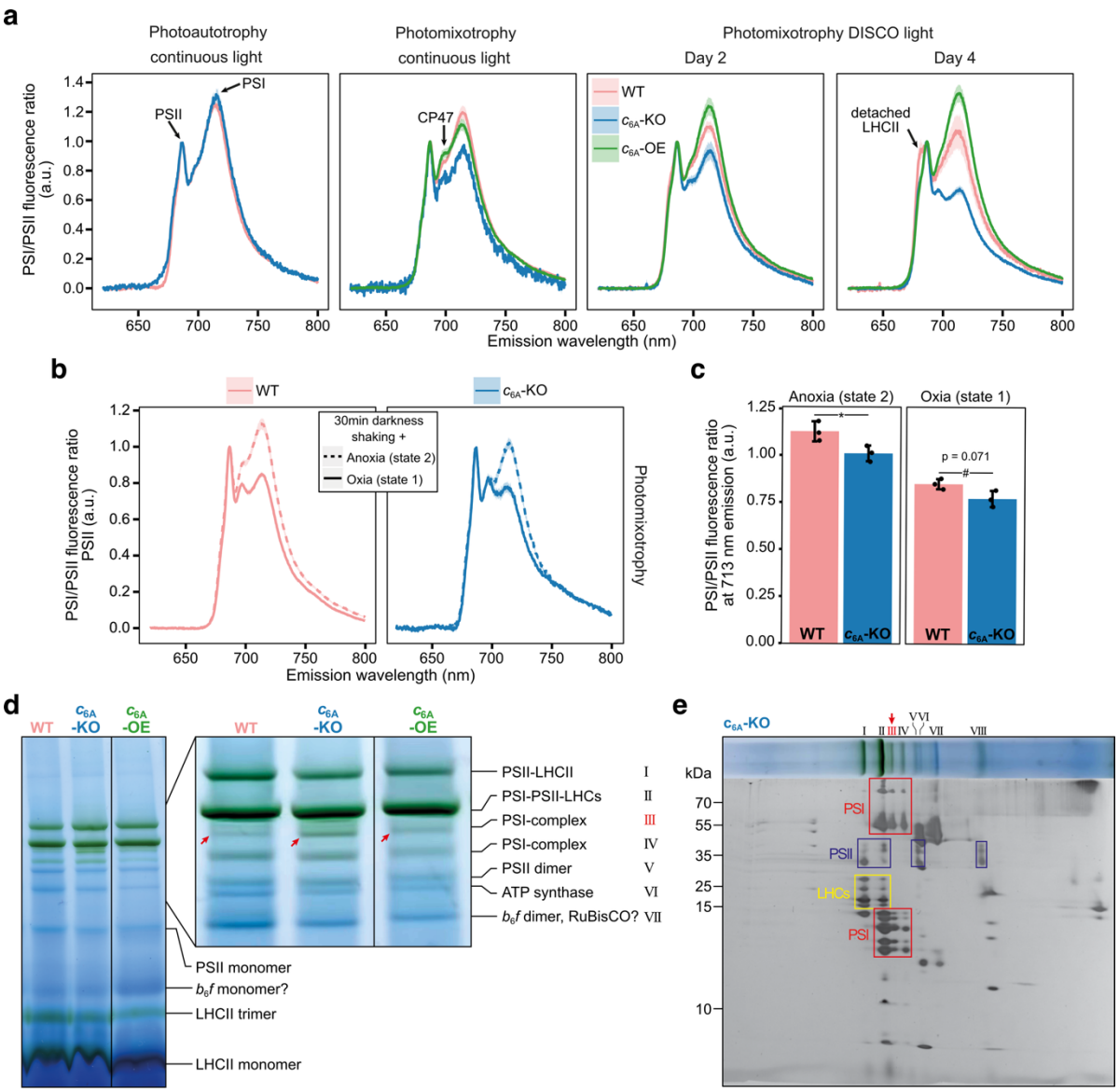

Figure 2: c_{6A} affects the light harvesting balance between photosystems I and II in photomixotrophy. a, Low temperature (77 K) chlorophyll fluorescence spectra (excitation: 440 nm) of c_{6A} mutant strains and WT from cells grown under continuous light (30 $\mu mol_{photons}\ m^{-2}\ s^{-1}$) in photoautotrophy -or mixotrophy and cells grown photomixotrophically under DISCO Light for 2 or 4 days. The prominent PSI and PSII fluorescence peaks of note are indicated by black arrows. **b**, Low temperature (77 K) chlorophyll fluorescence spectra of c_{6A}-KO and WT exposed to state 1 or 2 inducing conditions (n = 3 biological replicates ±SE). **c**, Quantification of the PSI to PSII fluorescence ratio at 713 nm from **b**. Statistical testing was carried out with a two-sided t-test per state ($p < 0.05$: *, $p < 0.1$: #). **d**, BN-PAGE analysis of c_{6A} mutant strains and WT thylakoid membrane complexes isolated from cells grown in photomixotrophy and continuous light (30 $\mu mol_{photons}\ m^{-2}\ s^{-1}$). The inset shows the area of interest with band III from a separate longer BN-PAGE run with the same samples. The full gels with three biological replicates per strain can be found in Supplementary Figure 6. Thylakoid membrane complexes were assigned to bands according to the literature (36–38). **e,** 2D-PAGE analysis of a BN-PAGE lane from c_{6A}-KO with the boxes indicating assignment of spots to protein complexes based on comparison with calculated R_f values of known thylakoid membrane complex components (Supplementary Fig. 7c).

As the light harvesting balance is affected by photosystem complex abundance and composition, we next analyzed the thylakoid membrane complexes from cells grown in standard conditions using BN-PAGE. Gels showed a distinct green band containing a PSI complex without LHCs (band III marked red, Fig. 2d&e) that was consistently more prominent in c_{6A}-KO compared to WT and c_{6A}-OE. The

240 other bands showed a similar pattern and thus presumably similar photosystem complex levels across
241 strains (Fig. 2d). 2D-PAGE analyses and gel simulations to calculate the predicted mobility in the gel
242 (R_f) revealed similar subunit compositions of the complexes between strains (Fig. 2e &
243 Supplementary Fig. 7a-b).

244 Together, these results show that c_{6A} is important for maintaining the light harvesting balance between
245 the photosystems in photomixotrophic conditions, especially in combination with DISCO light, and
246 indicate that an altered distribution of LHCs could underly this observation.

247

248 <u>Absence of c_{6A} leads to a more reduced PQ pool</u>
249 Given the tight link between light harvesting balance and the redox state of the PQ pool, we
250 quantified the redox state of the PQ pool using chlorophyll fluorescence measurements.

251 Firstly, the chlorophyll fluorescence induction (OJIP) traces of cells grown in standard conditions
252 revealed a 10% increase in the F_J parameter in c_{6A}-KO compared to WT and c_{6A}-OE ($P = 0.012$ and
253 0.008, respectively) (Fig. 3a,b). Since F_J reflects the extent of Q_A reduction and is positively
254 correlated with PQ pool reduction (39), this increase indicates that the absence of c_{6A} led to a more
255 reduced PQ pool.

256 To investigate further the extent of c_{6A}-dependent PQ pool overreduction, we exposed cells grown in
257 standard conditions to DISCO light and recorded chlorophyll fluorescence. The value of the steady-
258 state fluorescence yield F' under actinic light is influenced by the redox state of the PQ pool, as the
259 PQ pool is in a redox equilibrium with Q_A in PSII (40). During the high light periods of DISCO Light,
260 F' was on average 36% higher in c_{6A}-KO than in WT ($P = 0.0006$), indicating a more reduced PQ pool
261 in the absence of c_{6A} in DISCO Light as well (Fig. 3c). Also during the high light periods of the
262 DISCO Light regime, 1-qL (a measure of Q_A reduction) was high in WT (0.9) indicating that Q_A and
263 by implication the PQ pool was highly reduced (41). In c_{6A}-KO 1-qL was significantly higher (0.975)
264 again compared to WT ($P = 6.8 \times 10^{-5}$) (Fig. 3d), indicating a more reduced PQ pool, consistent with
265 the F' finding.

266 These results suggest that the absence of c_{6A} leads to a more reduced PQ pool in *Chlamydomonas*
267 under photomixotrophic conditions, exacerbated by DISCO Light exposure. Consequently, the more
268 reduced Q_A pool could lead to increased damage to PSII, potentially contributing to the observed
269 growth penalty in DISCO Light.

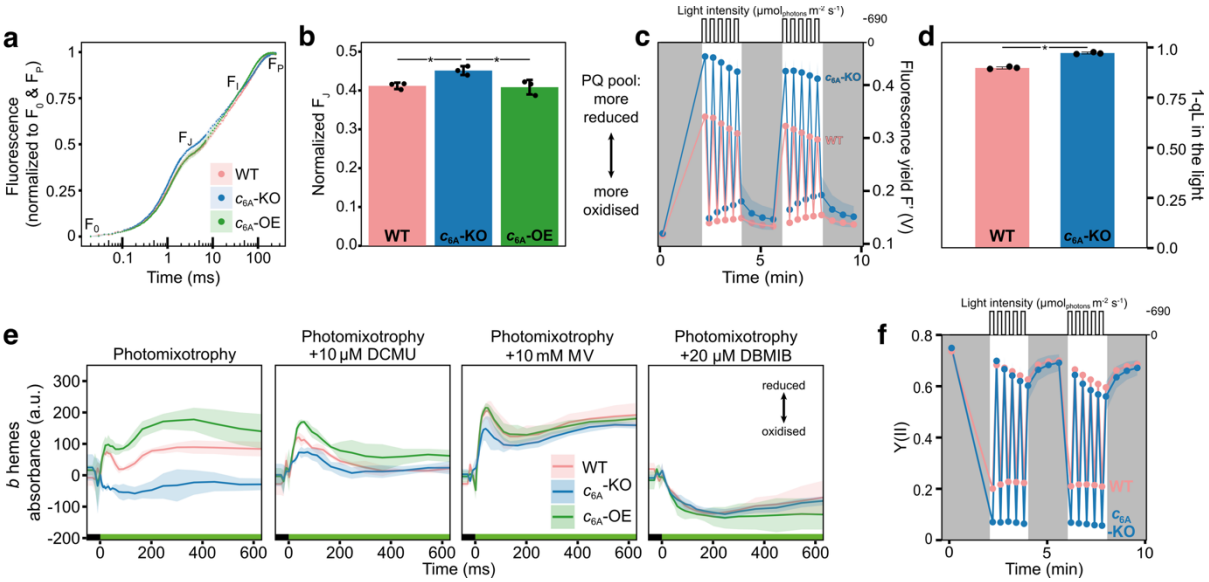

Figure 3: c_{6A} affects the redox state of the PQ pool, the redox kinetics of *b* hemes in cytochrome b_6f and the quantum yield of PSII. a, Chlorophyll fluorescence induction measurements (OJIP curves) of c_{6A} mutant strains and WT grown under photomixotrophic continuous light (30 $\mu mol_{photons}$ m^{-2} s^{-1}) conditions and normalized to F_0 and F_P (n = 3 biological replicates ±SD). **b**, Comparison of the normalized fluorescence at inflection point F_J (2.4 ms) from **a**. Asterisks indicate a significant difference ($p < 0.05$) as determined by one-way ANOVA and post-hoc pairwise two-sided t-test (n = 3 biological replicates ±SD). **c**, Raw steady-state fluorescence yield F' in Volts (V) of c_{6A}-KO and WT grown under standard conditions and exposed to a DISCO Light regime (on top of box) in a DUAL-PAM-100 spectrometer (n = 3 biological replicates ±SD). **d**, 1-qL values in the light phases of c_{6A}-KO and WT grown under standard conditions and exposed to the same light protocol as in **c** (n = 3 biological replicates ±SD, asterisk: significant difference ($p < 0.001$) as determined by two-sided t-test). **e**, Redox changes of *b* hemes in c_{6A} mutant strains and WT grown under standard conditions and exposed to DCMU (competitive inhibitor of the Q_B site in PSII), methyl viologen (MV, electron acceptor of PSI) or dibromothymoquinone (DBMIB, b_6f Q_P site blocker). Samples were exposed to green light (500 $\mu mol_{photons}$ m^{-2} s^{-1}, green bar) in a JTS-10 spectrometer (n = 3 biological replicates ±SD). **f**, Photosystem II quantum yield, Y(II), of c_{6A}-KO and WT grown under standard conditions and exposed to the same light protocol as in **c** (n = 3 biological replicates ±SD).

<u>Redox kinetics of *b* hemes are affected and PSII quantum yield lowered in absence of c_{6A}</u>

Given the effects of the absence of c_{6A} on light harvesting and PQ pool redox balance, we also assessed the function of PETC complexes. We first measured the redox kinetics of cytochrome b_6f using a Joliot-type spectrometer (JTS).

In photoautotrophic samples grown under continuous light (30 $\mu mol_{photons}$ m^{-2} s^{-1}), all strains exhibited a *b* hemes reduction peak within 100 ms of light exposure, but in c_{6A}-KO the peak was only half the intensity of WT (Supplementary Fig. 8). In samples grown in standard photomixotrophic conditions, the *b* hemes in WT and c_{6A}-OE were reduced within 100 ms of light exposure followed by transient oxidation and re-reduction. In contrast, the *b* hemes in c_{6A}-KO were *oxidized* within 100 ms of illumination (Fig. 3e) and showed nearly no re-reduction in the following 500 ms. Interestingly, no differences in the cytochrome *f* redox kinetics were observed in either photoautotrophy or photomixotrophy (Supplementary Fig. 8), indicating no effect of the absence of c_{6A} on the function of the high potential chain.

299 A more reduced PQ pool leads to lower reduction and even apparent oxidation of the *b* hemes upon
300 light exposure (42–44). The latter is likely due to *b* hemes being pre-reduced in conditions with a
301 highly reduced PQ pool. Thus, the effect of the absence of c_{6A} on the redox kinetics of b hemes are
302 consistent with the observed change in the redox state of the PQ pool. Artificial modulation of the PQ
303 pool redox state should therefore lead to smaller differences in *b* hemes redox kinetics between the
304 strains. In the presence of dichlorophenyl-dimethylurea (DCMU), a PSII inhibitor that leads to PQ
305 pool oxidation, samples grown in standard conditions showed that the *b* hemes in c_{6A}-KO were indeed
306 reduced upon illumination but to a lower magnitude than in WT/ c_{6A}-OE (Fig. 3e). Similarly, when we
307 added methyl viologen (MV), an artificial electron acceptor from PSI that also leads to PQ pool
308 oxidation, the *b* hemes reduction was partially restored in in c_{6A}-KO (Fig. 3e). Furthermore, when we
309 added dibromothymoquinone (DBMIB), which blocks the Q_P site of cytochrome b_6f and leads to PQ
310 pool reduction, the *b* hemes only showed oxidation upon illumination without differences between the
311 strains (Fig. 3e).

312 The observed differences in *b* hemes redox kinetics can therefore be explained by the more reduced
313 PQ pool in c_{6A}-KO. Further, these results indicate that in the absence of c_{6A} the cytochrome b_6f
314 complex including the Q-cycle is in principle functional if the PQ pool is oxidized. Nevertheless,
315 small differences between c_{6A}-KO and WT/ c_{6A}-OE remained when the PQ pool was artificially
316 oxidized, warranting further investigation of the Q-cycle.

317

318 To investigate the possibility of a disturbed Q-cycle underlying the *b* hemes phenotype, we measured
319 the proton motive force (*pmf*) and its components of *Chlamydomonas* cells grown in standard
320 conditions using electrochromic shift (ECS) measurements. No substantial difference between
321 presence and absence of c_{6A} was detected in *pmf*, proton flux (vH^+) and thylakoid conductivity (gH^+)
322 when samples were exposed to either continuous red light (53 $\mu mol_{photons}\ m^{-2}\ s^{-1}$) or DISCO Light
323 conditions (Supplementary Fig. 9a-f). Further, no differences between the strains were found in the
324 response of the ECS signal to a single turnover flash and the partitioning of *pmf* into ΔpH and ΔΨ
325 (Supplementary Fig. 9g&h). Together, this is consistent with c_{6A} not affecting Q-cycle function.

326

327 We also analyzed the efficiency of photosystems I and II of *Chlamydomonas* cells grown in standard
328 conditions when exposed to continuous or DISCO Light. In continuous light, we did not find any
329 significant differences between WT and c_{6A}-KO in the quantum yield of PSII (Supplementary Fig.
330 10a) and PSI (Supplementary Fig. 10b) over a wide range of intensities. There was, however, elevated
331 photosystem II quantum yield Y(II) for c_{6A}-OE in comparison to c_{6A}-KO at higher light intensities
332 (above 210 $\mu mol_{photons}\ s^{-1}\ m^{-2}$) resulting in an increased relative electron transport rate (rETRII).
333 Conversely, during the high light periods of DISCO Light, Y(II) was less than half in c_{6A}-KO

334 compared to WT (Fig. 3f). In contrast to PSII, PSI quantum yield Y(I) was not majorly affected by
335 absence of c_{6A} and DISCO Light and showed a decreasing trend in the light phases from 0.2 to about
336 0.125 over the course of 40 min in both WT and c_{6A}-KO (Supplementary Fig. 11). For both strains,
337 DISCO Light led to an increase in acceptor side limitation Y(NA), indicating that in DISCO Light
338 downstream electron acceptors are not readily available (Supplementary Fig. 11). Consistent with the
339 more reduced PQ pool in absence of c_{6A}, c_{6A}-KO exhibited a lower donor-side limitation Y(ND) than
340 WT during DISCO Light treatment (Supplementary Fig. 11).

341 The DISCO Light condition therefore seems to lead to inhibition of photosynthesis at PSII in c_{6A}-KO
342 which is consistent with the highly reduced PQ pool in absence of c_{6A}.

343

344 c_{6A} partly alleviates the stressful effect of DISCO Light on PSII
345 To determine if the more reduced PQ pool in the absence of c_{6A} causes stress for *Chlamydomonas* and
346 could explain the observed growth phenotype, we measured PSII energy partitioning of cells grown in
347 standard conditions and then exposed to DISCO Light using a DUAL-PAM.

348 Increased stress levels in the absence of c_{6A} were evident when examining the quantum yield of non-
349 regulated dissipation of excitation energy, Y(NO), which describes the fraction of energy that is
350 neither used for photochemistry nor dissipated as heat in a regulated manner via NPQ. At the start of
351 DISCO Light exposure, over 90% of light energy was dissipated in a non-regulated fashion in c_{6A}-
352 KO, while WT had values below 80% (Fig. 4a). Over 40 minutes of DISCO Light, Y(NO) levels in
353 c_{6A}-KO relaxed, nearing WT levels of about 70%. High Y(NO) levels indicate PSII photoinhibition
354 that is imminent or has already occurred due to over-reduction (45). When probing for PsbA, C-
355 terminal fragments forming two bands at around 15 kDa were visible (Fig. 4b). An increased ratio of
356 PsbA (D1) degradation products to full length PsbA (D1) protein, which is indicative of PSII
357 photoinhibition (46), was observed in c_{6A}-KO on Day 4 of DISCO Light exposure (Fig. 4b &
358 Supplementary Fig. 12). In c_{6A}-KO, 20% of the observed PsbA (D1) protein signal originated from the
359 C-terminal fragment bands, while in WT and c_{6A}-OE the C-terminal fragments only contributed 8%
360 and 7% to the total PsbA (D1) signal, respectively (Supplementary Fig. 12).

361 The yield of regulated non-photochemical quenching Y(NPQ) was negligible in dark-adapted WT and
362 c_{6A}-KO samples (Fig. 4b). However, over the first 40 min of DISCO Light exposure, c_{6A}-KO
363 exhibited approximately twice the Y(NPQ) levels as WT during all phases of the DISCO Light
364 protocol. This sustained Y(NPQ) response, even in the dark, indicates increased stress levels in the
365 absence of c_{6A}, leading to an amplified engagement of NPQ mechanisms to allow energy dissipation
366 in a regulated manner. Interestingly, increased Y(NPQ) in the absence of c_{6A} was also observed under
367 a range of continuous light intensities, which was partially restored in the c_{6A}-OE strain
368 (Supplementary Fig. 10a). Elevated NPQ levels in the absence of c_{6A} were further supported by an

approximately 1.5-fold protein level of the NPQ effector LHCSR3 (47) in c_{6A}-KO compared to WT after two days of growth in DISCO Light (Fig. 4b & Supplementary Fig. 12).

Together, these data indicate that PSII experiences more photoinhibition in c_{6A}-KO than WT and c_{6A}-OE under DISCO Light consistent with the observed reduced Y(II) in c_{6A}-KO under DISCO Light (Fig. 3f). Increased photoinhibition is likely contributing to the observed growth penalty (Fig. 1c).

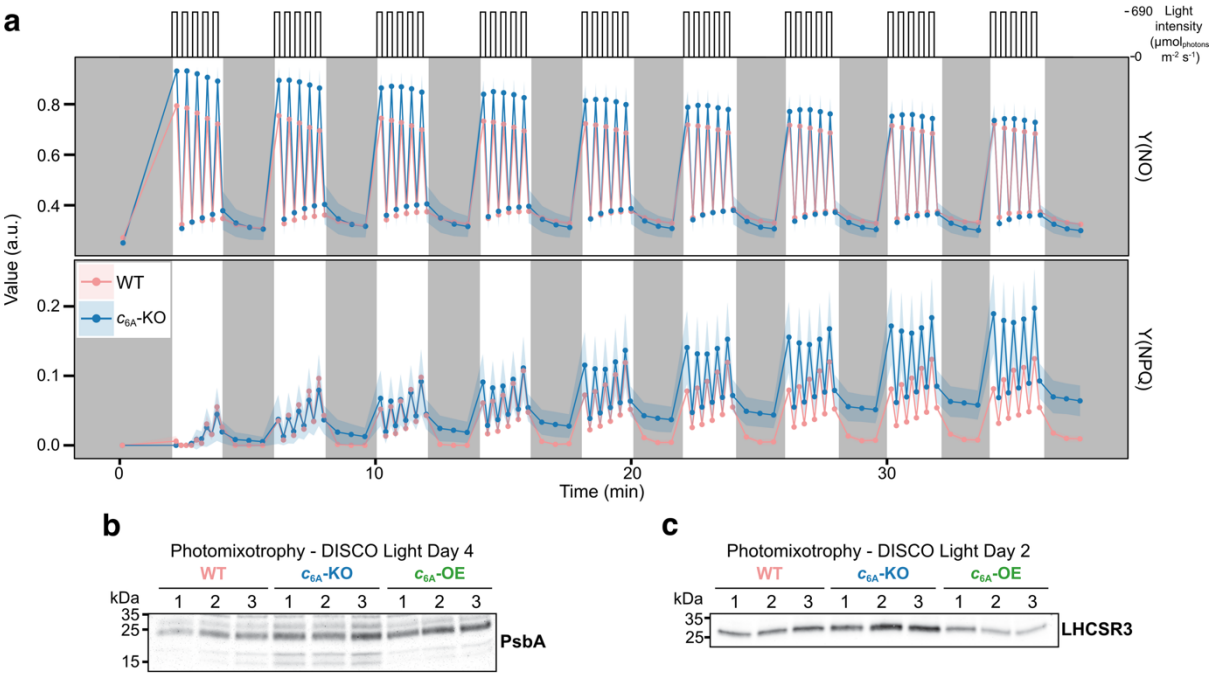

Figure 4: c_{6A} partly alleviates the stressful effect of DISCO Light on *Chlamydomonas*. a, Regulated non-photochemical quenching Y(NPQ), and non-regulated energy dissipation Y(NO) of c_{6A}-KO and WT grown under standard conditions and exposed to a DISCO Light regime in a DUAL-PAM-100 spectrometer (n = 3 biological replicates ±SD). **b**, Immunoblot analyses probing for PsbA in whole cell protein samples from c_{6A} mutant strains and WT grown in DISCO Light for four days (n = 3 biological replicates). **c**, Immunoblot analyses probing for LHCSR3 in whole cell protein samples from c_{6A} mutant strains and WT grown in DISCO Light for two days (n = 3 biological replicates). Relative quantification of the share of signal from C-terminal fragments for PsbA or the signal intensities normalized to total protein for LHCSR3 and can be found in Supplementary Figure 12.

Discussion

Here we present an in-depth characterization of the physiological role of the highly conserved cytochrome c_{6A} protein in relation to photosynthesis and show that it is important for optimal growth in fluctuating light due to its effect on the light harvesting and PQ pool redox state balances of the model alga *Chlamydomonas* (summary see Supplementary Table 1).

Analysis of the redox state of the PQ pool using complementary chlorophyll fluorescence approaches indicated that the PQ pool was more reduced in c_{6A}-KO, and this was particularly marked in the high light periods of DISCO Light. JTS measurements of the redox state of the *b* hemes of the cytochrome b_6f complex in response to light exposure showed disturbance of the redox kinetics in the c_{6A}-KO that were consistent with a more reduced PQ pool in c_{6A}-KO. Addition of DCMU or MV, which would be

394 expected to lead to PQ oxidation, or DBMIB, which leads to PQ reduction, revealed effects consistent
395 with an increased pre-reduction of the *b* hemes in c_{6A}-KO through a more reduced PQ pool. c_{6A}-KO
396 exhibited no change in the proton motive force, measured by electrochromic shift, rendering unlikely
397 a direct effect of c_{6A} on the Q cycle. Under the high light periods of DISCO Light, c_{6A}-KO showed a
398 dramatic decrease in PSII quantum yield compared to WT, which would also be consistent with a
399 more reduced PQ pool. The c_{6A}-KO did not exhibit any significant difference in PSI quantum yield
400 under DISCO light, although it showed a decrease in donor-side limitation of PSI, again consistent
401 with a more reduced PQ pool. c_{6A}-KO also showed some indication of increased acceptor-side
402 limitation.

403 c_{6A}-KO exhibited an increase in the non-regulated dissipation of excitation energy [Y(NO)] and
404 regulated non-photochemical quenching [Y(NPQ)] with the onset of DISCO Light, as well as a
405 relative increase in the amount of the NPQ effector LHCSR3 protein and degradation products of
406 PsbA after two and four days of growth in DISCO Light, respectively. These results indicate an
407 increased tendency to photoinhibition in c_{6A}-KO, which might be accounted for by the increased PQ
408 reduction. A general impairment of PSII function or repair in the absence of any other effects from
409 loss of c_{6A} might be expected to lead to a decreased reduction in PQ. This suggests that the PSII
410 impairment is a consequence of the increased PQ reduction resulting from loss of c_{6A}, rather than the
411 primary result of c_{6A} loss.

412 What might cause the increase in reduction of the PQ pool in the absence of c_{6A}? The 77K chlorophyll
413 fluorescence data indicated a significantly lower PSI/PSII fluorescence ratio in c_{6A}-KO compared to
414 WT under photomixotrophic conditions, and this difference was amplified under DISCO Light
415 conditions. In BN-PAGE, a band corresponding to a LHC-less PSI was more prominent in c_{6A}-KO
416 than WT and c_{6A}-KO showed a lower PSI/PSII fluorescence value than the wild type under both state
417 1 and state 2 conditions. These data are consistent with the photosystems being preferentially in the
418 equivalent of state 1 in c_{6A}-KO compared to WT. However, there was no evidence for the c_{6A}-KO
419 being permanently 'locked' in either state 1 or state 2.

420 Overall, it therefore seems likely that c_{6A}-KO is disturbed in the light harvesting balance between PSI
421 and PSII, in favor of PSII, especially under DISCO Light. This leads to a more reduced PQ pool, and
422 consequent photoinhibition, with impaired growth of c_{6A}-KO in DISCO conditions. c_{6A} is likely to be
423 located in the thylakoid lumen and has been shown to interact with the lumen thiol oxidase LTO1
424 (21), which is closely involved in thiol-based regulation of the STT7 (STN7 in Arabidopsis) state
425 transition kinase, keeping STT7 oxidized (22). STT7 is active only when oxidized and, in response to
426 a reduced PQ pool, catalyzes phosphorylation of LHCII and causing LHCII to move from PSII to PSI.
427 c_{6A} has been proposed to catalyze the formation of disulfide bridges in the lumen (10, 11), transferring
428 electrons to plastocyanin, with which it has been shown to react (19). Although we cannot exclude a

429 more complex explanation, with the shift in PSI/PSII balance and change in state of the PQ pool being
430 indirect consequences of loss of c_{6A}, we propose that c_{6A} contributes to oxidation of STT7. c_{6A} is not
431 essential for the oxidation as state transitions remain in c_{6A}-KO. However, it may be that c_{6A} assists in
432 the transfer of electrons from STT7 to LTO1 (with which it interacts (21)) or another acceptor. Thus,
433 in the absence of c_{6A}, STT7 would be more reduced than in WT, leading to increased light harvesting
434 at PSII and a more reduced PQ pool compared to WT. This model could be tested in the future by
435 making substitutions to the conserved cysteine residues in c_{6A}. If correct, this will be a significant
436 contribution to our understanding of the complex thiol-based regulatory network of the thylakoid
437 lumen of photosynthetic organisms (48). Furthermore, the demonstration of the importance of c_{6A} for
438 growth under fluctuating light conditions presents a significant contribution to understand how
439 organisms cope with rapidly changing light conditions (49, 50). The connection of c_{6A} to state
440 transitions also make it a significant target for optimizing crop productivity.

441

442 **Methods**

443 Growth conditions

444 *Chlamydomonas* strains were maintained on Tris-Acetate-Phosphate (TAP) (51) medium with
445 Hutner's trace element solution (52) supplemented with 1.5% agar at 30 $\mu mol_{photons}\ m^{-2}\ s^{-1}$ and 25 °C.
446 For longer-term storage cultures were kept on TAP slants in ambient light at room temperature. Liquid
447 cultures were grown at 30 $\mu mol_{photons}\ m^{-2}\ s^{-1}$, 25 °C and 120 rpm in AlgaeTron AG130 or AG230
448 incubators (Photon System Instruments) unless otherwise specified.

449 For experimental cultures, triplicates of 30 mL medium (Tris-phosphate (TP) medium (51) for
450 photoautotrophic, and TAP for photomixotrophic conditions) were inoculated with *Chlamydomonas*
451 strains to OD_{750nm} = 0.1. The cultures were then subjected to the experimental conditions (Table 1).
452 All experimental cultures were subcultured at least twice in standard conditions before exposure to
453 experimental conditions.

454 Table 1: Experimental light conditions in the AlgaeTron AG130 and AG230 growth chambers.

Name	**Light regime**
Standard growth light	continuous 30 $\mu mol_{photons}\ m^{-2}\ s^{-1}$
High light	continuous 700 $\mu mol_{photons}\ m^{-2}\ s^{-1}$
Darkness	continuous 0 $\mu mol_{photons}\ m^{-2}\ s^{-1}$
2 min on/off	alternating 2 min 700 $\mu mol_{photons}\ m^{-2}\ s^{-1}$ & 2 min darkness
12 s on/off	alternating 12 s 700 $\mu mol_{photons}\ m^{-2}\ s^{-1}$ & 12 s darkness
DISCO Light	alternating 2 min darkness & 2 min of 12 s 700 $\mu mol_{photons}\ m^{-2}\ s^{-1}$/ 12 s off (Fig. 1d)

455

456 Algal strains

457 The cytochrome c_{6A} knock-out strain "c_{6A}-KO" (CC-1883 background) was generated as previously
458 described (32) using the gRNAs 5'-ATTTACAGTTAGTGCATCCACTTG-3' and 5'-
459 TCCGAGGGTAAGCAAGCACGGCAC-3' to target the 5'UTR and Exon III for Cpf1-mediated
460 double strand breaks, respectively. A repair template with the following sequence was provided at the
461 same time to introduce a multiple stop codon (lowercase letters): 5'-
462 TCATGCTCGGCCAGTTTTCTTTGATTTCAAATCCTCGCTAATTTActaattaactaaCAGCTTCCTT
463 GCTTCATGGACCCAGTAACGGTGCATGGGTACGCG-3'. The knock-out in the strain "c_{6A}-KO"
464 was confirmed through whole locus PCR, showing a truncated locus in the c_{6A}-KO strain compared to
465 WT (Supplementary Fig. 1b). Sanger sequencing validated the deletion of the *CYC4* sequence from
466 5'UTR to exon III and the introduction of a sequence with multiple stop codons. Whole genome
467 sequencing with high read depth in both strains showed the c_{6A} locus was disrupted in the targeted
468 region in c_{6A}-KO but not in WT (Supplementary Fig. 1c). Transcriptomic analysis showed no c_{6A} gene
469 transcripts in the c_{6A}-KO strain, indicating effective disruption of transcription (Supplementary
470 Fig. 1d).

471 The c_{6A}-overexpression strain c_{6A}-OE was created by transforming c_{6A}-KO with the constructs
472 pDKM-000 by electroporation as described before (53) with the following specifications. A
473 *Chlamydomonas* culture from standard growth conditions with OD_{750} ~ 1 was concentrated 100-fold in
474 TAP with 60 mM sucrose. 250 µL were then incubated with 1 µg of linearized DNA (PmeI) for 10
475 min on ice in an electroporation cuvette (0.4 cm gap, BioRad) prior to electroporation (BioRad Gene
476 Pulser). Cells were recovered in 10 mL TAP with 60 mM sucrose for 16 h in a shaking incubator (2
477 µmol photon m^{-2} s^{-1}, 120 rpm, 25°C) prior to plating for selection on TAP-agar plates with
478 Paromomycin (10 µg/mL). Following selection, immunoblot analysis confirmed the expression of
479 c_{6A}-FLAG in three PCR-confirmed transformants, showing a band just under 15 kDa, which
480 corresponds well to the expected size of c_{6A}-FLAG without its predicted signal peptide (13.5 kDa, cut
481 site VLA/AEA, TargetP2.0) (Supplementary Fig. 1e). One colony (number 3 in Supplementary Fig.
482 1e) was selected as the representative c_{6A}-OE strain. RNAseq analysis showed a ~14-fold increase in
483 c_{6A} transcripts compared to WT, confirming overexpression (Supplementary Fig. 1d).

484 The construct pDKM-000 was assembled following the molecular cloning syntax with the parts
485 pCM0-016 (PSAD promoter) (53), pDK0-002 (*CYC4* gene with introns, this study), pCM0-094 (C-
486 terminal triple FLAG tag) (53), and pCM0-114 (PSAD terminator) (53). The *CYC4* gene coding for
487 c_{6A} with two intronic BsaI restriction sites altered (GAGACC→GAAACC) was synthesized (Twist
488 Bioscience).

489

490 PCR genotyping and whole genome sequencing

491 The genotype regarding the *CYC4* allele of the strains used was determined using the Phire Plant
492 Direct PCR kit (Thermo Fisher) and following the manufacturer's instructions. Primers were used that
493 spanned the whole c_{6A} gene binding 245 bp upstream and 75 bp downstream of *CYC4* (fw: 5'-
494 GAGACGCTACGCTGCATGT-3' & rev: 5'-ACTTCCTCGCGCTGCATA-3', annealing: 65 °C,
495 extension: 45 s). For WT, this should lead to an amplicon of 2469 bp while for c_{6A}-KO a 1773 bp
496 amplicon is expected, following the CRISPR induced deletion of 708 bp and addition of a 12 bp
497 multiple stop codon.
498 For the confirmation of transformation with pDKM-000, colony PCR with the primers spanning the
499 transgene was performed as above (fw: 5'-TCTTTCTCCATGGGCGGGCT-3', rev: 5'-
500 CCCTCGGTCACATGTGCATCC-3', annealing: 69 °C, extension: 70 s).

501 For whole genome sequencing, genomic DNA from photomixotrophically grown cultures under
502 standard conditions was obtained by phenol:chloroform extraction. The DNA was found to be of
503 sufficient quality via spectrophotometric quantification (NanoDrop) and gel electrophoresis and was
504 subsequently subjected to Illumina sequencing (PE-150 technology, Novogene, Cambridge, UK).
505 After confirming the quality of the raw reads using FastQC (54), BBDuk in Geneious Prime was used
506 to trim adapter sequences, low quality (< 30 quality value) and short reads (<10 bp). Subsequently,
507 reads were aligned to the latest reference genome assembly for *Chlamydomonas* from JGI (CC-4532
508 v6.1 (55)) with the Geneious Mapper. Coverages of 97.8% (WT) and 97.4% (c_{6A}-KO) were reached
509 with average read depths of 133.6x (WT) and 72.5x (c_{6A}-KO), and average mean MAPQ values of
510 202.3 (WT) and 200.3 (c_{6A}-KO). Integrative genomics viewer was used for coverage visualization
511 (56).

512

513 RNA sequencing

514 Mid-exponential phase *Chlamydomonas* cultures (5 mL) were harvested by centrifugation at 1000 xg
515 for 5 min. After disposal of the supernatant the cell concentrate was snap-frozen in liquid nitrogen.
516 The frozen pellet was resuspended in 1 mL of TRIzol reagent (Thermo Fisher Scientific) and stored
517 until further use at -80 °C. The TRIzol suspension was mixed with 1 mL of ethanol in preparation for
518 RNA purification using the Direct-zol RNA Miniprep kit (Zymo Research) following the
519 manufacturer's instructions. The optional DNase treatment and two additional wash steps were
520 included: one wash with 0.4 mL of RNA Wash Buffer before the DNase treatment and another wash
521 with 0.4 mL of Direct-zol RNA PreWash Buffer after the first pre-wash. The resulting concentrations
522 and the 260/280, 260/230 ratios were subsequently quantified spectrophotometrically
523 (NanoDrop1000, Thermo Fisher Scientific). Integrity of the extracted RNA was confirmed by gel
524 electrophoresis.

525 The RNA samples were sent to Novogene for quality control, directional poly-A enriching library
526 preparation, and Illumina sequencing (PE-150 technology). After confirming the quality of raw reads
527 using FastQC (54), the latest genome assembly for *Chlamydomonas* from JGI (CC-4532 v6.1 (55))
528 was used as reference genome onto which raw reads were mapped with hisat2 (57). Alignment was
529 confirmed (between 82 and 95% aligned reads for all samples) and read assignment statistics were
530 calculated with picard tools (58). Count data for genetic features was extracted using featureCounts
531 (59) and the latest gff3 reference file for *Chlamydomonas* from JGI. The featureCounts table was
532 analyzed in R, where analysis of differential expression was performed with DEseq2 (60).

533

534 Chlorophyll quantification

535 A 200 µL sample from a *Chlamydomonas* culture was mixed with 800 µL acetone, vigorously mixed
536 for 20 s and centrifuged for 3 min at 13000 xg. The supernatant was isolated and its absorbance at 663
537 nm and 645 nm was measured against an 80% acetone blank. The concentration of chlorophyll a, b
538 and total chlorophyll was calculated with the dilution factor D (here D = 5) as Chl a (µg/mL) = (OD_{663}
539 $*12.7 - OD_{645} *2.69) *D$; Chl b (µg/mL) = ($OD_{645} *22.9 - OD_{663} *4.68) *D$; Total chl (µg/mL)= chl a
540 + chl b (61).

541

542 Protein extraction and Western Blot

543 A known volume of *Chlamydomonas* cells at a desired growth stage was harvested by centrifugation
544 at 1000 xg for 5 min. The pellet was subsequently resuspended in RIPA lysis buffer with freshly
545 added PMSF (1mM final concentration) to reach a calculated OD_{750nm} of 50. The chlorophyll content
546 was measured as above, but here 10 µL of sample were mixed with 40 µL of acetone and 1 mL of
547 80% acetone, resulting in a dilution factor D of 105. Protein samples were then adjusted to the same
548 total chlorophyll concentration with RIPA buffer and frozen at -20 °C for at least 1.5 h or overnight,
549 followed by thawing on ice to complete cell lysis. Protein concentration was determined using a
550 Bradford assay (Merck) according to manufacturer's instructions diluting the protein samples 5- to
551 10-fold.

552 For SDS-PAGE, all samples were diluted to 1 µg/µL protein with RIPA buffer before being mixed
553 with 4x Lämmli buffer and incubated for 30 min (50 °C, 600 rpm). After centrifuging the samples
554 (12000 xg, 1 min) to remove insoluble material, samples were loaded to the desired amount into wells
555 of polyacrylamide gels (Mini-PROTEAN TGX Stain-Free, BioRad). PageRuler Plus (7 µL, Thermo
556 Scientific) was used as size marker. Electrophoresis was carried out at 4 °C and 200 V for about 50
557 min. The gel was imaged in a ChemiDoc MP imaging system (BioRad) using the Stain Free setting
558 and 5 min activation time. Some gels were stained with Pierce™ Silver Stain for Mass Spectrometry
559 (Thermo Scientific).

560 Transfer of protein from polyacrylamide gels onto polyvinylidene fluoride (PVDF) membranes was
561 carried out using the iBlot dry transfer apparatus, following the manufacturer's instructions and using
562 program P3 for 5 min. Membranes were then probed for successful transfer with PonceauS (Thermo
563 Scientific) as per manufacturer's instructions and imaged with the ChemiDoc MP imaging system
564 (BioRad). Following the PonceauS destaining, membranes were blocked in 5% milk in Tris-buffered
565 saline with 0.1% Tween 20 (TBS-T) for 1 h at room temperature with gentle shaking. After washing
566 membranes once with TBS-T to remove remnants of blocking agent, membranes were incubated with
567 specific primary antibody solutions in 5% milk TBS-T overnight at 4 °C (PsaB (AS10695, Agrisera)
568 at 1:1000, PsbA D1 (AS05084, Agrisera) at 1:10000, LHCSR3 (AS142766, Agrisera) at 1:2000).
569 Subsequently, membranes were washed with TBS-T (5x 5 min) and incubated for 1.5 h at room
570 temperature with goat anti-rabbit horseradish peroxidase-linked secondary antibody in 5% milk TBS-
571 T (1:10000, 1706515, BioRad). After washing membranes thrice in TBS-T and once in TBS (10 min
572 each), they were incubated with chemiluminescence substrate (SuperSignal™ West Pico PLUS
573 Chemiluminescent Substrate, Thermo Scientific) and imaged using a ChemiDoc MP imaging system
574 (BioRad).

575

576 Low temperature chlorophyll (77K) fluorescence

577 77K fluorescence emission spectra were recorded with a QE Pro spectrophotometer (Ocean Optics,
578 Dunedin, FL, USA). Cell samples (200 µL) frozen in liquid N_2 were excited with blue light (440 nm).
579 Raw spectra were normalized to the photosystem II (PSII) fluorescence peak at 685 nm.

580 *Chlamydomonas* cells were harvested and total chlorophyll concentration was adjusted to 5 µg/mL
581 with fresh medium (TP or TAP). Cells were then frozen in liquid N_2 for measurement.

582 For the state transition experiment, *Chlamydomonas* cells grown in TAP under standard conditions
583 were adjusted to 5 µg/mL total chlorophyll with fresh medium. Anoxia (state 2 inducing) samples
584 were adjusted with medium containing glucose (final concentration 20 mM) and Glucose Oxidase
585 (final concentration 50 U/mL) that was purged with N2 for 3 min. The final samples were again
586 purged with N_2 before being sealed. Oxia (state 1 inducing) samples were adjusted with unchanged
587 medium and left unsealed. All samples were then shaken for 30 min in darkness before being frozen
588 in liquid N_2 for fluorescence measurement.

589

590 Blue native PAGE and second dimension SDS-PAGE

591 Thylakoid membranes from *Chlamydomonas* cultures were isolated over a discontinuous Percoll
592 gradient as described before (62). BN-PAGE was then carried out largely as previously (63).
593 Thylakoid samples were diluted with resuspension buffer (25 mM Bis-Tris/HCl (pH 7.0), 20% (w/v)

594 glycerol, 0.25 mg/ml Pefabloc, and 10 mM sodium fluoride) to a chlorophyll concentration of 0.53
595 µg/µL and to a total of 6 µg chlorophyll. An equal volume of β -dodecyl maltoside (β -DM, 2% in
596 resuspension buffer) was added to each sample and the thylakoid membranes were solubilized by
597 gentle pipetting for 2 min. After centrifugation (4 °C, 18000 xg, 20 min) samples were mixed with a
598 one-tenth volume of sample loading buffer (100 mM Bis-Tris/HCl (pH 7.0), 0.5 M ACA, 30% (w/v)
599 sucrose and 50 mg/ml Serva Blue G) and loaded into the wells of a NativePAGE 3-12% Bis-Tris
600 protein gel (Invitrogen). Electrophoresis was carried out with specific anode buffer (50 mM Bis-
601 Tris/HCl, pH 7.0) and cathode buffer containing Serva Blue G dye (50 mM Tricine, 15 mM Bis-
602 Tris/HCl, pH 7.0, and 0.01% Serva Blue G) at 4 °C for 20 min at 75 V, 30 min at 100 V, 30 min at
603 125 V, 60 min at 150 V, 30 min at 175 V and 60 min at 200 V. After the 30 min at 125 V, the blue
604 cathode buffer was replaced by the same cathode buffer but without Serva Blue G. The last step was
605 prolonged to 5 h if additional separation of bands of interest was needed.

606 Gel electrophoretic separation of complexes in BN-PAGE lanes on a second dimension SDS-PAGE
607 was carried out as previously described (63, 64), although 12% polyacrylamide gels were used here.
608 Gels were stained with Pierce™ Silver Stain (Thermo Scientific).

609 The predicted mobility in the gel (R_f) values of known thylakoid membrane complex components
610 were calculated using their known molecular weight and a linear regression of the distance of the
611 protein standard in relation to the running front ($r^2 = 0.98$). The 2D-PAGE spots were compared with
612 the R_f values and with published BN-PAGE analyses from *Chlamydomonas* (36–38) to assign the
613 bands and proteins.

614

615 Chlorophyll fluorescence

616 Chlorophyll fluorescence induction (OJIP) of *Chlamydomonas* was measured with a FL3500
617 fluorometer (Photon System Instruments). Prior to measurement, cells were resuspended in TAP and
618 total chlorophyll concentration was adjusted to 20 µg/mL. After recovery under standard growth
619 conditions for at least 30 min, chlorophyll concentration was readjusted to 5 µg/mL. After 15 min
620 incubation in darkness, fluorescence induction in response to red light (984 $\mu mol_{photons}\ m^{-2}\ s^{-1}$, 45% A-
621 voltage) was recorded for 120 s. Raw fluorescence data was double normalized to fluorescence at
622 time point 0 and the maximum fluorescence value to compare the kinetics between samples (41).

623 Chlorophyll fluorescence of *Chlamydomonas* was measured with a pulse amplitude-modulated
624 spectrometer (Dual-PAM-100, Walz). Prior to measurements, cells were resuspended in TAP and the
625 chlorophyll concentration was adjusted to 20 µg/mL. After recovery under standard growth conditions
626 for at least 30 min, measurements were performed in a quartz cuvette at 25 °C with stirring and
627 samples were initially incubated in darkness for 5 min before the blue fluorescence measuring light
628 (Intensity 12, 28 $\mu mol_{photons}\ m^{-2}\ s^{-1}$) was turned on. Saturating pulses (Intensity 5, 5000 $\mu mol_{photons}\ m^{-2}$

629 s^{-1}, 500 ms width) for PSII parameter determination were applied with stirring turned off. DISCO
630 Light conditions in the DUAL-PAM-100 were achieved by alternating 2 min darkness followed by 2
631 min consisting of 12 s high light (690 $\mu mol_{photons}$ m^{-2} s^{-1}) and 12 s darkness alternations. Saturating
632 pulses were applied in the middle of each 12 s phase or three times during the 2 min dark phases. F'
633 was recorded as the fluorescence yield during illumination with the actinic light treatment before
634 application of a saturating pulse. Photosynthetic parameters were calculated as described previously
635 (45).

636

637 P700 redox measurements

638 Simultaneous whole-cell P700 absorbance and chlorophyll fluorescence of *Chlamydomonas*
639 (Supplementary Figure 10) were measured with a pulse amplitude-modulated spectrometer (Dual-
640 PAM-100, Walz). Prior to measurements, cells were resuspended in TAP and the total chlorophyll
641 concentration was adjusted to 20 µg/mL. After recovery under standard growth conditions for at least
642 30 min, 2 mL of the cell suspension were filtered onto glass fiber filters (WHA1822025, Whatman)
643 and 100 µL fresh TAP were added to keep the filter moist. Measurements were performed using leaf
644 clamps holding the filter and samples were initially incubated in darkness for 5 min before
645 fluorescence (Intensity 12, 28 $\mu mol_{photons}$ m^{-2} s^{-1}) and P700 measuring light (Intensity 15) were turned
646 on.

647 Saturating pulses (Intensity 5, 5000 $\mu mol_{photons}$ m^{-2} s^{-1}, 500 ms width) were applied that allowed
648 calculation of photosynthetic parameters as before (45, 65) with P700 SP-evaluation settings adjusted
649 to 7 ms delay and 10 ms width.

650

651 Cytochrome b_6f redox kinetics

652 Cytochrome *f* and *b* heme redox kinetics were determined in *Chlamydomonas* cells by deconvoluting
653 absorbance changes at 546, 554, 563, and 573 nm that were measured using a JTS-10 pump probe
654 spectrophotometer (BioLogic) and appropriate 10 nm FWHM (full width at half maximum)
655 interference filters (Edmund Optics). BG39 filters (Schott) were used to shield the light detectors from
656 scattered light. Prior to measurements, cells were resuspended in fresh medium to a total chlorophyll
657 concentration of 20 µg/mL. After recovery under standard growth conditions for at least 30 min,
658 Ficoll 400 was added to a final concentration of 10%. For some samples, DCMU, methyl viologen, or
659 DBMIB were added to a final concentration of 10 µM, 10 mM, or 20 µM respectively, at the same
660 time as Ficoll. Cells were dark-adapted for 3 min before measurement with each interference filter
661 and then illuminated with 5 s of green light (500 $\mu mol_{photons}$ m^{-2} s^{-1}). Flashes of white detection light
662 were administered during 300 µs dark intervals in actinic illumination. Every recording was corrected
663 for any detection light impact by subtracting a trace with actinic light turned off. Deconvolution was

performed with the JTS-10 software by drawing a baseline between 573 and 546 nm. During analysis, the signal-to-noise ratio was improved with a Savitzky-Golay filter (66).

Immunofluorescence microscopy

Immunofluorescence staining of *Chlamydomonas* cells was carried out as previously described (67), however the methanol incubation step was left out to retain chlorophyll in the samples serving as a thylakoid marker. The antibodies used were primary mouse anti-FLAG (1:2500, B3111, Sigma) and secondary goat anti-Mouse IgG Alexa Fluor™ 488 (1:200, A11029, Invitrogen).

An inverted fluorescence microscope (Nikon Eclipse Ti) was used to investigate the stained slides. Brightfield and epifluorescence images were taken with a 20X or 100X oil immersion lens. AlexaFluor 488 signal was recorded in a YFP channel (500 nm excitation (73% intensity), yellow emission filter, 500 ms exposure) while another channel was used for chlorophyll autofluorescence (635 nm excitation (31% intensity), red emission filter, 500 ms exposure). Images were acquired as z-stacks (acquisition every 0.3 µm) and the fluorescence signals were deconvoluted using the Richardson-Lucy method and 20 iterations in the NIS-Elements Advanced Research Software (Nikon).

Co-immunoprecipitation

Chlamydomonas cultures from mid exponential growth phase were harvested by centrifugation (1000 xg, 5 min) and the pellets were resuspended in RIPA lysis buffer with freshly added PMSF (1 mM final concentration) and DNAse I (final concentration 100 U/mL). Cells were lysed by bead-beating (~100 µL of 425-600 µm beads) for 5 cycles of 1 min bead-beating and 1 min on ice. The lysate was pelleted (1 min, 2000 xg) before the supernatant was centrifuged again for 5 min at 15000 xg. The cleared lysate was then diluted with dilution buffer (10 mM Tris/Cl pH 7.5, 150 mM NaCl, 0.5 mM EDTA) and protein concentration was determined with a Bradford assay. For co-immunoprecipitation of FLAG-tagged proteins and putative interaction partners in the lysates, DYKDDDDK Fab-Trap™ Agarose beads (Chromotek) were utilized as per manufacturer's instructions with at least 4 washes and elution with 2x SDS sample buffer. For the co-immunoprecipitation of samples grown in standard conditions, a different colony than number 3 but containing the same construct (pDKM-000) was used.

Electrochromic shift measurements of proton motive force

Changes in the proton motive force and components, vH+ and gH+, were determined with a Dual-PAM-100 (Walz) by measuring absorbance difference signal at the 550-515 nm, known as

electrochromic shift (ECS) (68). Dark interval relaxation kinetics (DIRKs) were recorded by interrupting actinic light exposure for 450 ms with darkness. Prior to measurements, *Chlamydomonas* cells were resuspended in fresh medium and the total chlorophyll concentration was adjusted to 20 µg/mL. After recovery under standard growth conditions for at least 30 min, Ficoll 400 was added to a final concentration of 10%. Cells were dark-adapted for 10 min before measurement and measurements started with a single turnover flash (100 µs) used later for normalization of the ECS signal. For the standard growth condition induction experiment red actinic light (53 $\mu mol_{photons}\ m^{-2}\ s^{-1}$) was turned on and DIRKs recorded every 5 s for 30 s and every 10 s thereafter. For the DISCO Light experiment the light regime as in described in the PSII/PSI parameter measurements section was used, but instead of saturating pulses, DIRKs were recorded. At the end of the protocol, slow relaxation of the ECS signal in darkness was recorded for 1 min and used later for analysis of partitioning the pmf into ΔpH and ΔΨ (69). Analysis of kinetic data was carried out using OriginPro (Version 2024, OriginLab Corporation). The first 20 ms of the DIRK were fitted with a linear regression, the absolute slope of which corresponds to the proton flux (vH+) (70), while the inverse of the time constant of the first order exponential decay fit of a DIRK corresponds to the activity of the thylakoid conductivity (gH+) (71). ECS signals were normalized to the ECS magnitude induced by a single-turnover saturating flash of 20 µs in dark-adapted cells.

References

1. M. Weigel, *et al.*, Plastocyanin is indispensable for photosynthetic electron flow in Arabidopsis thaliana. *J. Biol. Chem.* **278**, 31286–31289 (2003).
2. G. A. Peschek, C. Obinger, M. Paumann, The respiratory chain of blue-green algae (cyanobacteria). *Physiol. Plant.* **120**, 358–369 (2004).
3. R. Gupta, Z. He, S. Luan, Functional relationship of cytochrome c6 and plastocyanin in Arabidopsis. *Nature* **417**, 567–571 (2002).
4. J. Wastl, D. S. Bendall, C. J. Howe, Higher plants contain a modified cytochrome c6. *Trends Plant Sci.* **7**, 244–245 (2002).
5. J. Wastl, S. Purton, D. S. Bendall, C. J. Howe, Two forms of cytochrome c6 in a single eukaryote. *Trends Plant Sci.* **9**, 474–476 (2004).
6. I. Nimmo, Location and function of cytochrome c6A. *PhD Thesis Univ. Camb.* (2011).
7. C. J. Howe, R. H. Nimmo, A. C. Barbrook, D. S. Bendall, "Cytochrome c6A of Chloroplasts" in *Cytochrome Complexes: Evolution Structures, Energy Transduction and Signaling*, Advances in Photosynthesis and Respiration., W. A. Cramer, T. Kallas, Eds. (Springer Science+Business Media, 2016).
8. U. Hani, *et al.*, A complex and dynamic redox network regulates oxygen reduction at photosystem I in Arabidopsis. *Plant Physiol.* (2024). https://doi.org/10.1093/plphys/kiae501.
9. B. A. Slater, The ancestry and function of cytochrome c6A. *PhD Thesis Univ. Camb.* (2020).
10. C. J. Howe, B. G. Schlarb-Ridley, J. Wastl, S. Purton, D. S. Bendall, The novel cytochrome c6 of chloroplasts: a case of evolutionary bricolage? *J. Exp. Bot.* **57**, 13–22 (2006).
11. B. G. Schlarb-Ridley, R. H. Nimmo, S. Purton, C. J. Howe, D. S. Bendall, Cytochrome c 6A is a funnel for thiol oxidation in the thylakoid lumen. *FEBS Lett.* **580**, 2166–2169 (2006).
12. H. Chida, *et al.*, Crystal structure of oxidized cytochrome c 6A from Arabidopsis thaliana. *FEBS Lett.* **580**, 3763–3768 (2006).

13. J. A. R. Worrall, B. F. Luisi, B. G. Schlarb-Ridley, D. S. Bendall, C. J. Howe, Cytochrome c 6A: discovery, structure and properties responsible for its low haem redox potential. *Biochem. Soc. Trans.* **36**, 1175–1179 (2008).
14. J. M. Mason, D. S. Bendall, C. J. Howe, J. A. R. Worrall, The role of a disulfide bridge in the stability and folding kinetics of Arabidopsis thaliana cytochrome c6A. *Biochim. Biophys. Acta BBA - Proteins Proteomics* **1824**, 311–318 (2012).
15. J. A. R. Worrall, *et al.*, Modulation of Heme Redox Potential in the Cytochrome c 6 Family. *J. Am. Chem. Soc.* **129**, 9468–9475 (2007).
16. B. Slater, D. Kosmützky, R. E. R. Nisbet, C. J. Howe, The Evolution of the Cytochrome c6 Family of Photosynthetic Electron Transfer Proteins. *Genome Biol. Evol.* **13**, 1–12 (2021).
17. F. P. Molina-Heredia, *et al.*, A new function for an old cytochrome? *Nature* **424**, 33–34 (2003).
18. J. Wastl, *et al.*, Redox properties of Arabidopsis cytochrome c6 are independent of the loop extension specific to higher plants. *Biochim. Biophys. Acta BBA - Bioenerg.* **1657**, 115–120 (2004).
19. M. J. Marcaida, *et al.*, Structure of Cytochrome c6A, a Novel Dithio-cytochrome of Arabidopsis thaliana, and its Reactivity with Plastocyanin: Implications for Function. *J. Mol. Biol.* **360**, 968–977 (2006).
20. P. Pesaresi, *et al.*, Mutants, overexpressors, and interactors of arabidopsis plastocyanin isoforms: Revised roles of plastocyanin in photosynthetic electron flow and thylakoid redox state. *Mol. Plant* **2**, 236–248 (2009).
21. Y. Lu, *et al.*, Identification of Potential Targets for Thylakoid Oxidoreductase AtVKOR/LTO1 in Chloroplasts. *Protein Pept. Lett.* **22**, 219–225 (2015).
22. J. Wu, *et al.*, Functional redox links between lumen thiol oxidoreductase1 and serine/threonine-protein kinase STN7. *Plant Physiol.* **186**, 964–976 (2021).
23. P. J. Gollan, A. Trotta, A. A. Bajwa, I. Mancini, E.-M. Aro, Characterization of the Free and Membrane-Associated Fractions of the Thylakoid Lumen Proteome in Arabidopsis thaliana. *Int. J. Mol. Sci.* **22**, 8126 (2021).
24. J. Beltrán, *et al.*, Specialized Plastids Trigger Tissue-Specific Signaling for Systemic Stress Response in Plants. *Plant Physiol.* **178**, 672–683 (2018).
25. M. Janssen, *et al.*, Efficiency of light utilization of Chlamydomonas reinhardtii under medium-duration light/dark cycles. *J. Biotechnol.* **78**, 123–137 (2000).
26. P. J. Graham, B. Nguyen, T. Burdyny, D. Sinton, A penalty on photosynthetic growth in fluctuating light. *Sci. Rep.* **7**, 1–11 (2017).
27. L. Nikkanen, *et al.*, PGR5 is needed for redox-dependent regulation of ATP synthase both in chloroplasts and in cyanobacteria. [Preprint] (2024). Available at: http://biorxiv.org/lookup/doi/10.1101/2024.11.03.621747 [Accessed 27 August 2025].
28. M. Jokel, X. Johnson, G. Peltier, E. Aro, Y. Allahverdiyeva, Hunting the main player enabling Chlamydomonas reinhardtii growth under fluctuating light. *Plant J.* **94**, 822–835 (2018).
29. C. J. Steen, A. Burlacot, A. H. Short, K. K. Niyogi, G. R. Fleming, Interplay between LHCSR proteins and state transitions governs the NPQ response in Chlamydomonas during light fluctuations. *Plant Cell Environ.* **45**, 2428–2445 (2022).
30. T. Roach, LHCSR3-Type NPQ Prevents Photoinhibition and Slowed Growth under Fluctuating Light in Chlamydomonas reinhardtii. *Plants* **9**, 1604 (2020).
31. W. J. Nawrocki, *et al.*, Chlororespiration Controls Growth Under Intermittent Light. *Plant Physiol.* **179**, 630–639 (2019).
32. A. Ferenczi, D. E. Pyott, A. Xipnitou, A. Molnar, Efficient targeted DNA editing and replacement in Chlamydomonas reinhardtii using Cpf1 ribonucleoproteins and single-stranded DNA. *Proc. Natl. Acad. Sci.* **114**, 13567–13572 (2017).
33. C. A. Kerfeld, H. P. Anwar, R. Interrante, S. Merchant, T. O. Yeates, The Structure of Chloroplast Cytochromec6at 1.9 Å Resolution: Evidence for Functional Oligomerization. *J. Mol. Biol.* **250**, 627–647 (1995).
34. E. G. Andrizhiyevskaya, *et al.*, Origin of the F685 and F695 fluorescence in Photosystem II. *Photosynth. Res.* **84**, 173–180 (2005).

35. J. Kargul, J. Nield, J. Barber, Three-dimensional reconstruction of a light-harvesting complex I-photosystem I (LHCI-PSI) supercomplex from the green alga Chlamydomonas reinhardtii: Insights into light harvesting for PSI. *J. Biol. Chem.* **278**, 16135–16141 (2003).
36. E. Devadasu, *et al.*, Long- and short-term acclimation of the photosynthetic apparatus to salinity in Chlamydomonas reinhardtii. The role of Stt7 protein kinase. *Front. Plant Sci.* **14**, 1–17 (2023).
37. J. G. García-Cerdán, *et al.*, A thylakoid membrane-bound and redox-active rubredoxin (RBD1) functions in de novo assembly and repair of photosystem II. *Proc. Natl. Acad. Sci. U. S. A.* **116**, 16631–16640 (2019).
38. B. Spaniol, *et al.*, Complexome profiling on the Chlamydomonas lpa2 mutant reveals insights into PSII biogenesis and new PSII associated proteins. *J. Exp. Bot.* **73**, 245–262 (2022).
39. S. Z. Tóth, G. Schansker, R. J. Strasser, A non-invasive assay of the plastoquinone pool redox state based on the OJIP-transient. *Photosynth. Res.* **93**, 193 (2007).
40. B. A. Diner, Dependence of the deactivation reactions of Photosystem II on the redox state of plastoquinone pool a varied under anaerobic conditions. Equilibria on the acceptor side of Photosystem II. *Biochim. Biophys. Acta BBA - Bioenerg.* **460**, 247–258 (1977).
41. H. M. Kalaji, *et al.*, Frequently asked questions about chlorophyll fluorescence, the sequel. *Photosynth. Res.* **132**, 13–66 (2017).
42. P. Joliot, A. Joliot, Proton pumping and electron transfer in the cytochrome bf complex of algae. *Biochim. Biophys. Acta BBA - Bioenerg.* **849**, 211–222 (1986).
43. F. Buchert, M. Scholz, M. Hippler, Electron transfer via cytochrome b 6 f complex displays sensitivity to antimycin A upon STT7 kinase activation. *Biochem. J.* **479**, 111–127 (2022).
44. A. Malnoë, F.-A. Wollman, C. de Vitry, F. Rappaport, Photosynthetic growth despite a broken Q-cycle. *Nat. Commun.* **2**, 301 (2011).
45. C. Klughammer, U. Schreiber, Complementary PS II quantum yields calculated from simple fluorescence parameters measured by PAM fluorometry and the Saturation Pulse method. *PAM Appl. Notes* **1**, 27–35 (2008).
46. W. J. Nawrocki, *et al.*, Molecular origins of induction and loss of photoinhibition-related energy dissipation q I. *Sci. Adv.* **7**, 1–13 (2021).
47. M. Ballottari, *et al.*, Identification of pH-sensing Sites in the Light Harvesting Complex Stress-related 3 Protein Essential for Triggering Non-photochemical Quenching in Chlamydomonas reinhardtii. *J. Biol. Chem.* **291**, 7334–7346 (2016).
48. D. Hoh, J. E. Froehlich, D. M. Kramer, Redox regulation in chloroplast thylakoid lumen: The pmf changes everything, again. *Plant Cell Environ.* **47**, 2749–2765 (2024).
49. N. A. Eckardt, *et al.*, Lighting the way: Compelling open questions in photosynthesis research. *Plant Cell* **14**, 1–16 (2024).
50. S. P. Long, *et al.*, Into the Shadows and Back into Sunlight: Photosynthesis in Fluctuating Light. *Annu. Rev. Plant Biol.* **73**, 617–648 (2022).
51. D. S. Gorman, R. P. Levine, Cytochrome f and plastocyanin: their sequence in the photosynthetic electron transport chain of Chlamydomonas reinhardi. *Proc. Natl. Acad. Sci.* **54**, 1665–1669 (1965).
52. S. H. Hutner, L. Provasoli, A. Schnatz, C. P. Haskins, Some Approaches to the Study of the Role of Metals in the Metabolism of Microorganisms. *Proc. Am. Philos. Soc.* **94**, 152–170 (1950).
53. P. Crozet, *et al.*, Birth of a Photosynthetic Chassis: A MoClo Toolkit Enabling Synthetic Biology in the Microalga *Chlamydomonas reinhardtii*. *ACS Synth. Biol.* **7**, 2074–2086 (2018).
54. S. Andrews, FastQC: A Quality Control Tool for High Throughput Sequence Data. (2010). Available at: http://www.bioinformatics.babraham.ac.uk/projects/fastqc/.
55. R. J. Craig, *et al.*, The Chlamydomonas Genome Project, version 6: Reference assemblies for mating-type plus and minus strains reveal extensive structural mutation in the laboratory. *Plant Cell* **35**, 644–672 (2023).
56. J. T. Robinson, *et al.*, Integrative genomics viewer. *Nat. Biotechnol.* **29**, 24–26 (2011).
57. D. Kim, J. M. Paggi, C. Park, C. Bennett, S. L. Salzberg, Graph-based genome alignment and genotyping with HISAT2 and HISAT-genotype. *Nat. Biotechnol.* **37**, 907–915 (2019). Available at: http://dx.doi.org/10.1038/s41587-019-0201-4.
58. Broad Institute, Picard Tools. Available at: http://broadinstitute.github.io/picard.

59. Y. Liao, G. K. Smyth, W. Shi, FeatureCounts: An efficient general purpose program for assigning sequence reads to genomic features. *Bioinformatics* **30**, 923–930 (2014).
60. M. I. Love, W. Huber, S. Anders, Moderated estimation of fold change and dispersion for RNA-seq data with DESeq2. *Genome Biol.* **15**, 1–21 (2014).
61. D. I. Arnon, COPPER ENZYMES IN ISOLATED CHLOROPLASTS. POLYPHENOLOXIDASE IN *BETA VULGARIS*. *Plant Physiol.* **24**, 1–15 (1949).
62. C. B. Mason, T. M. Bricker, J. V. Moroney, A rapid method for chloroplast isolation from the green alga Chlamydomonas reinhardtii. *Nat. Protoc.* **1**, 2227–2230 (2006).
63. S. Järvi, M. Suorsa, V. Paakkarinen, E. M. Aro, Optimized native gel systems for separation of thylakoid protein complexes: Novel super- and mega-complexes. *Biochem. J.* **439**, 207–214 (2011).
64. M. Rantala, V. Paakkarinen, E. M. Aro, Analysis of thylakoid membrane protein complexes by blue native gel electrophoresis. *J. Vis. Exp.* **2018**, 1–6 (2018).
65. C. Klughammer, U. Schreiber, Saturation Pulse method for assessment of energy conversion in PS I. *PAM Appl. Notes* 11–14 (2008).
66. M. J. E. Savitzky, A.; Golay, Smoothing and Differentiation of Data. *Anal Chem* **36**, 1627–1639 (1964).
67. T. Yamano, H. Fukuzawa, Indirect Immunofluorescence Assay in Chlamydomonas reinhardtii. *BIO-Protoc.* **6**, 1–6 (2016).
68. B. Bailleul, P. Cardol, C. Breyton, G. Finazzi, Electrochromism: A useful probe to study algal photosynthesis. *Photosynth. Res.* **106**, 179–189 (2010).
69. J. A. Cruz, C. A. Sacksteder, A. Kanazawa, D. M. Kramer, Contribution of electric field ($\Delta\psi$) to steady-state transthylakoid proton motive force (pmf) in vitro and in vivo. Control of pmf parsing into $\Delta\psi$ and ΔpH by ionic strength. *Biochemistry* **40**, 1226–1237 (2001).
70. P. Joliot, A. Joliot, Cyclic electron transfer in plant leaf. *Proc. Natl. Acad. Sci. U. S. A.* **99**, 10209–10214 (2002).
71. A. Kanazawa, D. M. Kramer, In vivo modulation of nonphotochemical exciton quenching (NPQ) by regulation of the chloroplast ATP synthase. *Proc. Natl. Acad. Sci. U. S. A.* **99**, 12789–12794 (2002).
72. S. Rexroth, J. M. W. Meyer zu Tittingdorf, F. Krause, N. A. Dencher, H. Seelert, Thylakoid membrane at altered metabolic state: Challenging the forgotten realms of the proteome. *Electrophoresis* **24**, 2814–2823 (2003).

Acknowledgements

We thank Dr. K. Geissler (University of Cambridge) for the provision of the pCM0 MoClo parts and Dr. J. Walter (University of Cambridge) for assistance with blue native PAGE. We are also grateful to Dr. M. Jokel (University of Turku) for discussions on cell culture. All photosynthesis experiments were performed within the PHOTOSYN infrastructure at the University of Turku. We gratefully acknowledge the support of this work by: the Gates Cambridge Trust with support from the Benn W Levy Trust, and the Professor John Glover Memorial Fund (to DK); the Novo Nordisk Foundation (PhotoCat, project no. NNF20OC0064371, to YA; and Photo-e-microbes project no. NNF22OCOO79717 to LTW); the Research Council of Finland no. 355335 to YA, (no. 354876) to LN; the Biotechnology and Biological Sciences Research Council (BB/M011194/1 to AS, BB/M011194/1 to JML, BB/R506163/1 to AF, and BB/Y001370/1 to CJH), and Trinity Hall, Cambridge (to JML).

Author contributions

DK conceived the project, designed and performed experiments under the supervision of CJH and YA, and analyzed data. DK, LTW, LN, and YA developed the biophysical part of the project. LTW and LN supervised the biophysical measurements and assisted with data analysis and interpretation. AF created the knock-out mutant line under the supervision of AM. JML and AS assisted with data

collection, analysis and interpretation. AM, YA, and CJH secured funding, assisted with data interpretation, and provided resources. DK wrote the manuscript with comments and input from all authors.

Competing interests

The authors declare no competing interests.